Motion of Light Adatoms and Molecules on the Surface of Few-Layer Graphene

Franziska Schäffel,*,† Mark Wilson,‡ and Jamie H. Warner†

†Department of Materials, University of Oxford, Parks Road, Oxford OX1 3PH, United Kingdom, and ‡Department of Chemistry, Physical and Theoretical Chemistry Laboratory, University of Oxford, South Parks Road, Oxford OX1 3QZ, United Kingdom

ABSTRACT

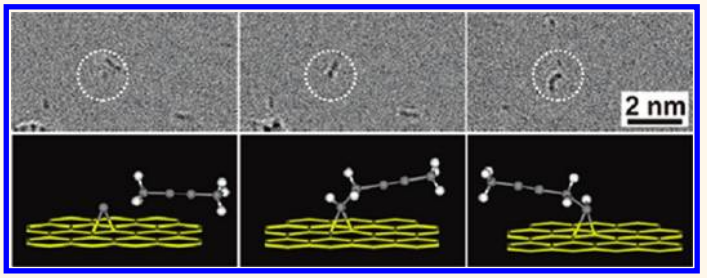

Low-voltage aberration-corrected transmission electron microscopy (TEM) is applied to investigate the feasibility of continuous electron beam cleaning of graphene and monitor the removal of residual species as present on few-layer graphene (FLG) surfaces. This combined approach allows us to detect light adatoms and evaluate their discontinuous sporadic motional behavior. Furthermore, the formation and dynamic behavior of isolated molecules on the FLG surface can be captured. The preferential source of adatoms and adsorbed molecules appeared to be carbonaceous clusters accumulated from residual solvents on the graphene surface. TEM image simulations provide potential detail on the observed molecular structures. Molecular dynamics simulations confirm the experimentally observed dynamics occurring on the energy scale imposed by the presence of the 80 kV electron beam and help elucidate the underlying mechanisms.

KEYWORDS: dynamic behavior of molecules · few-layer graphene · low-voltage transmission electron microscopy · TEM simulation · molecular dynamics computer simulation

Progress in the development of molecular-scale electronics, in particular the emergence of active components such as molecular switches or motors,[1] requires techniques that enable structural characterization of molecules and evaluation of their dynamics. Scanning probe techniques such as scanning tunnelling microscopy (STM) and atomic force microscopy (AFM) can obtain structural information on molecules on surfaces.[1−3] However, in order to resolve the molecular structure accurately, it is necessary to work at very low temperatures under ultra-high-vacuum conditions, and long measurement times are required due to the sequential nature of the scanning process.[2] Room-temperature acquisition of the dynamic behavior of molecules remains a challenge.

Transmission electron microscopy (TEM) is a direct technique with simultaneous image acquisition. The recent development of aberration correctors has pushed forward atomic-scale investigation of a large variety of materials and enabled the dynamical motion of molecular nanostructures to be examined.[4−7] Samples that are sensitive to high-energy electron radiation damage, so-called knock-on damage, can now be investigated at lower acceleration voltages without significant damage, which is highly relevant to carbon-based materials and molecules.[8]

Often TEM examination of molecular nanostructures has been carried out using cages, as for example carbon nanotubes, which are filled up with the molecules of interest. In this way fullerenes with and without functional groups have been studied extensively,[9−12] but also reactions and transformations of molecules in this confined space could be accessed.[6,13] Here, aberration-corrected low-voltage high-resolution transmission electron microscopy (LV-HRTEM) is unrivalled in terms of spatial resolution.[14] Using time series of HRTEM images the motional dynamics of molecules can be studied, revealing phenomena such as conformational changes and translational motion of organic molecules,[11,15,16] metallofullerenes performing rotational and translational movement within carbon nanotubes,[9,10] and oscillatory motion of nanotube fragments in a host nanotube.[17] Temporal resolution down to 80 ms can be achieved with HRTEM.[14] A powerful approach that provides improved temporal resolution is ultrafast electron microscopy (UEM), making use of pulsed electron sources.[18] However, the spatial resolution

* Address correspondence to franziska.schaeffel@materials.ox.ac.uk.

Received for review May 24, 2011 and accepted November 6, 2011.

Published online November 07, 2011
10.1021/nn2036494

of UEM is not sufficient to resolve the carbon−carbon distance and therefore is limited for investigation of individual carbon-based molecular nanomaterials.

HRTEM studies of adatoms and molecules on surfaces are rare. The recent developments in producing ultrathin two-dimensional membranes, for example graphene, graphene oxide, and boron nitride, as TEM supports have expedited HRTEM investigations of nanoparticles[19,20] and molecules.[21−25] This is due to the contrast of these membranes being uniform as well as very weak due to the limited number of atoms as compared to conventional amorphous carbon TEM support grids that usually have a thickness of 2−3 nm.[20,21] Furthermore, their highly ordered crystalline structure allows accurate calibration of the micrographs, and its contribution to the image can be removed *via* simple subtraction using masks in Fourier space.[19] Meyer *et al*. demonstrated that light atoms such as carbon and even hydrogen could be observed on graphene membranes by employing "only" a conventional HRTEM.[21] In order to improve the signal-to-noise ratio, the TEM micrographs were collected by summing multiple subsequent frames, leading to total acquisition times on the order of minutes. Within these time frames the authors reported on the dynamics of adsorbed molecules and the formation and healing of defects. In order to observe faster molecular motion at room temperature, single-shot TEM micrograph acquisition is necessary. Diffusion of metal atoms on graphene sheets has also been reported previously. For example, Au or Pt atom diffusion has been studied with *in situ* HRTEM.[26] Here the large mass difference of the metal atoms and the carbon support results in contrast from individual metal atoms and the ability to track their dynamic behavior. A recent example employing aberration-corrected LV-HRTEM was presented by Sloan *et al*., who studied the dynamics of polyoxometalate anions on graphene oxide with high precision.[24] These anions contain several tungsten atoms within the structure, which dominate the contrast through their strong scattering properties and allow for precise determination of the molecules' orientation with respect to the graphene oxide support.

A key component for the wide-scale uptake of using two-dimensional crystals, such as graphene, as supports for TEM studies is that the preparation method should be simple, straightforward, and reproducible by as many researchers as possible. Although mechanical exfoliation is very useful to identify single-layer-graphene (SLG) sheets, it involves many preparational steps including the characterization of graphite and graphene species using spectroscopy or atomic force microscopy prior to the actual transferral of the membrane onto a specialized TEM grid.[21] Substrate-free synthesis methods, for example, gas-phase-based[27] or solution-based methods,[28,29] represent an easier way to directly transfer SLG or few-layer graphene (FLG) sheets onto TEM grids. However, in all cases carbonaceous debris originating from the adhesive tape or the solvent coats the graphene surface and may obscure the image.

In this contribution we demonstrate and monitor the removal of such residual species present on a FLG surface derived from a standard solution-based preparation process *via* continuous electron irradiation. In order to prove the feasibility of the cleaning process, we further monitor and analyze the movement of atoms and molecules remaining "attached" to the clean FLG sheet. These adsorbates are subject to periods of fixed stability and after such a stable period rapidly move away or are sputtered off by the electron beam. Further, the dynamic behavior, *i.e*., the formation and motional dynamics of molecules consisting of light atoms—mainly carbon—on the FLG sheet, is detected. Details of the molecular structure are extracted, and insights gained through comparison with TEM image simulations. To understand the mechanistic origin of the observed motion, molecular dynamics computer simulations are performed using a relatively simple, well-established, potential model, allowing for the simulation of multiple adsorption events with the systematic variation of the key underlying control parameters such as the atom kinetic energy and its angle of approach.

RESULTS AND DISCUSSION

Graphene and FLG were prepared by liquid phase exfoliation using highly ordered pyrolytic graphite (HOPG) as graphite precursor and *N*-methyl-2-pyrrolidone (NMP) as solvent.[28] In brief, the solution was sonicated for 2 h and left to settle for 1 h. The top third of the dispersion was extracted for use, with the bottom two-thirds discarded. For TEM analysis a drop from the dispersion was deposited onto a lacey carbon TEM grid, washed in methanol, and then left to dry. The obtained graphene sheets typically comprised 1−10 graphene layers. Since HOPG is very clean compared to other graphite sources (metallic impurities <0.1 wt %) and since NMP contains only carbon, nitrogen, and oxygen atoms, residual species on the graphene flake's surface consist of only light atoms. LV-HRTEM was carried out using an aberration-corrected JEOL JEM-2200MCO transmission electron microscope, operated at an acceleration voltage of 80 kV to minimize knock-on damage.[30]

Figure 1a shows a TEM image of a typical FLG sheet consisting of six layers on a lacey carbon grid (*cf*. Supporting Information Figure S1 for determination of the number of layers). Figure 1b is taken from the region indicated with the red box in Figure 1a and shows that the surface of the FLG sheet is mostly covered with a thin layer of debris. This is attributed to residual NMP, amorphous carbon, and small graphene pieces arising from the sonication process and is typical for FLG samples. Figure 1c shows the same

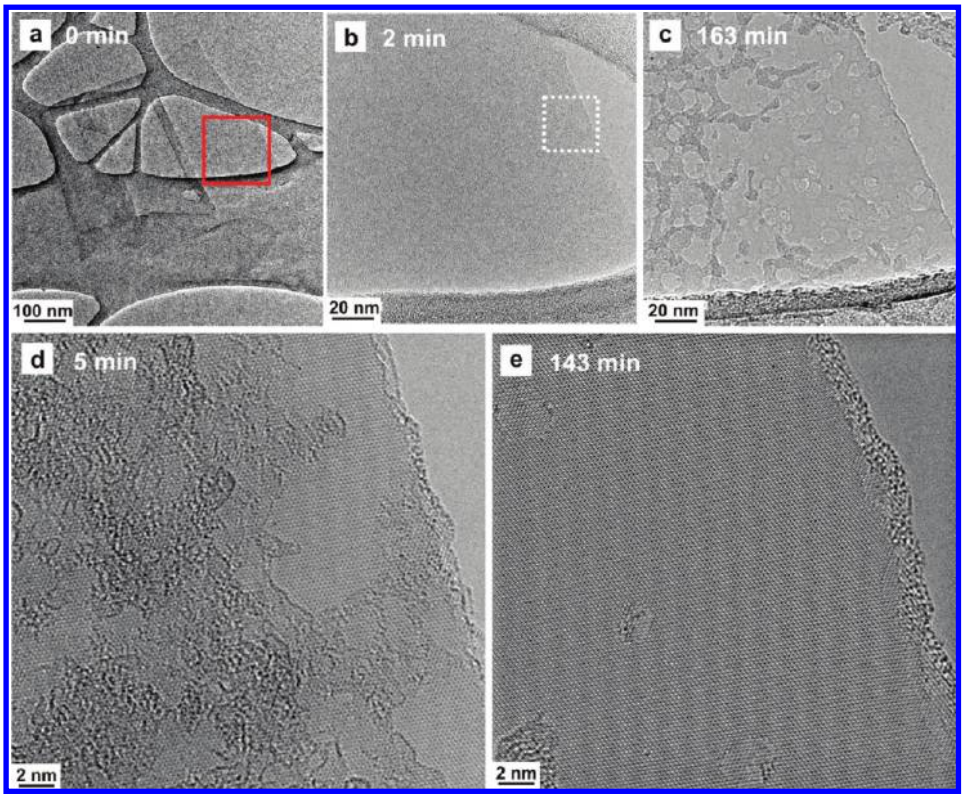

Figure 1. Cleaning graphene by means of electron beam irradiation (irradiation time indicated in each subfigure): (a) FLG flake; (b, c) TEM images of the graphene edge taken at a low magnification after 2 min (b) and after 163 min (c) electron irradiation. The more pronounced contrast in (c) arises from accumulation of surface species into clusters on the graphene sheet; (d, e) HRTEM images of the graphene sheet before (d) and after (e) electron irradiation. The latter shows a large area cleaned from adsorbates. These adsorbates collect in clusters, *cf.* (c) and bottom left in (e), or at the edge of the graphene sheet, which is now a lot wider than in (d).

region after 163 min of electron beam irradiation and the majority of the surface contamination has been removed from the irradiated area. Several circular voids were produced in the FLG sheet after the irradiation similar to previous observations, which is attributed to sputtering of carbon atoms surrounding defects and impurities.[14] Some areas with dark contrast are observed in Figure 1c; this more pronounced contrast arises from accumulation of surface species into larger clusters. High-resolution TEM micrographs before and after extensive electron beam irradiation of the region marked with a white square in Figure 1b are presented in Figure 1d,e. In Figure 1d, which was acquired very shortly after Figure 1b, a small amount of carbonaceous matter partially covers the surface of the FLG sheet. Figure 1e, acquired after an exposure time of 143 min, shows that the electron beam irradiation led to the residual material collecting in amorphous clusters on the surface of the FLG sheet (*cf.* Figure 1e, bottom left) as well as on the FLG edge, leaving large areas of the FLG sheet devoid of impurities. Typically, when electron beam irradiating a clean FLG edge, as seen in Figure 1d, edge atoms get sputtered off due to their lower binding energy.[14,31] However, the increase in "edge width", *i.e.*, the collection of amorphous material along the edge as observed here, indicates that surface migration events along the graphene plane (*xy*-plane) are feasible. Material from the top graphene surface, which is the side facing the electron source, is likely to be "kicked" toward the edge of the FLG sheet and/or the clusters through incoming high-energy electrons. For top surface atoms to be displaced into the FLG lattice, the so-called displacement energy has to be overcome.[32] The energy required to sputter an atom lying on the surface is much lower than that for atom displacement. It is further agreed that electron-beam-induced sputtering mainly affects the beam exit surface of a thin sample due to high-angle backscattered electrons transferring maximal momentum in a forward direction, *i.e.*, the direction of the incident electron beam.[33] Therefore, removal of material may preferentially occur from the back side of the sheet through electrons going through the FLG sheet and interacting with weakly bound matter on the back side. From our analysis of the reduction in surface area covered by the amorphous clusters with electron exposure time an approximate number of 8 atoms/s leaving the clusters was estimated (*cf.* Figure S2 in the Supporting Information).

A Fourier-enhanced image of the FLG sheet together with its fast Fourier transform (FFT) as an inset is shown in Figure 2a (see Supporting Information and Figure S3

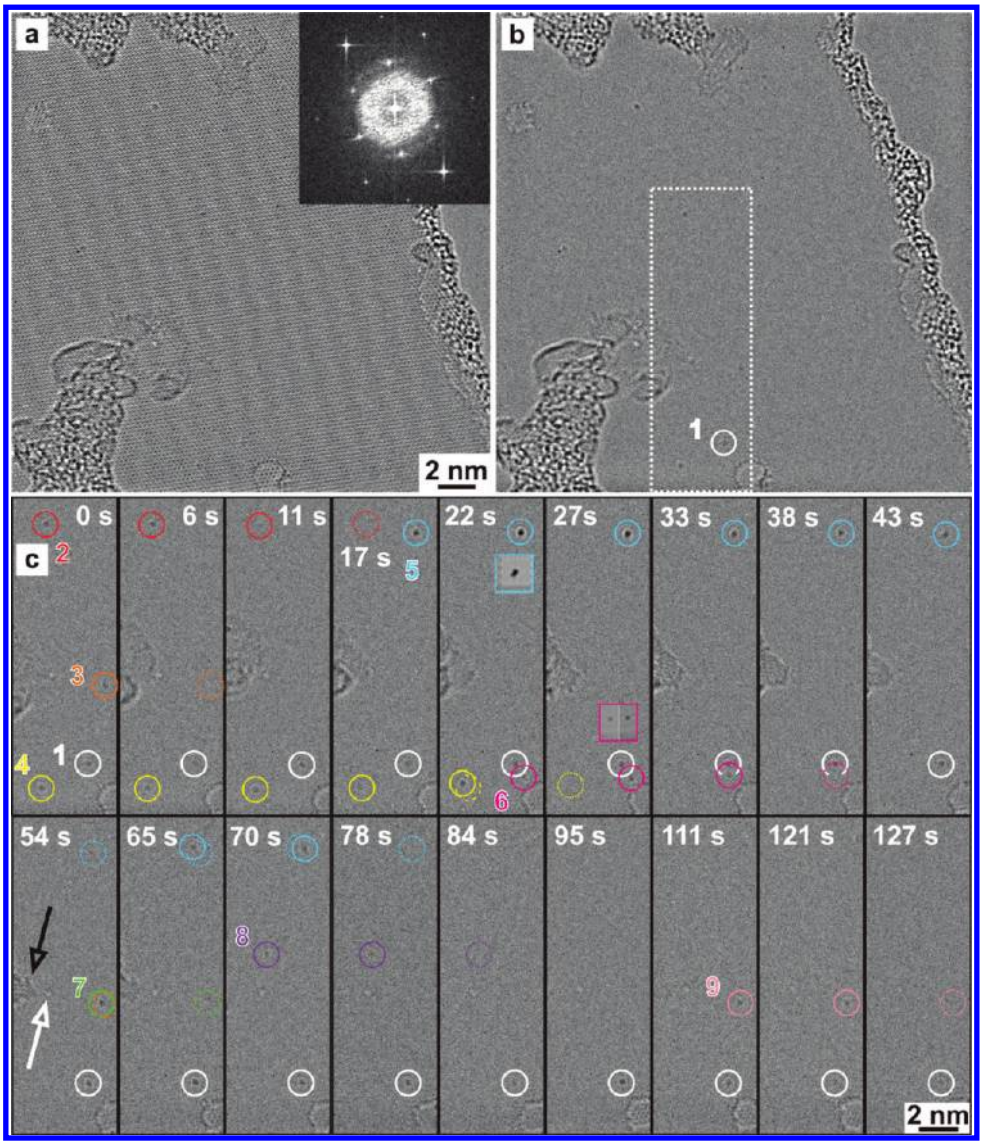

Figure 2. Adatoms appearing and disappearing on the FLG surface: (a) HRTEM image of the FLG flake including the respective FFT; (b) same HRTEM image as in (a) with FLG contrast subtracted from the image; (c) time sequence of the area marked white in (b). The image acquisition time for each frame was 1 s. Each individual feature is numbered and assigned a different color. They appear (full circles) and disappear (dotted circles) during the time sequence. Feature #1, marked with a white circle in (b) and all the images in (c), is stable during the whole period of time and thus acts as a positional reference. Note that the square insets in (c) after 22 and 27 s correspond to the appropriately scaled down image simulations of a carbon chain (22 s) and carbon adatoms (27 s), as will be discussed later.

for a detailed description of image processing). In Figure 2b the graphene contrast has been subtracted using a Fourier mask (*cf*. Figure S3) in order to enhance any deviations from the highly periodic graphene crystal structure, such as the sputtered edges of a layer, adsorbates, defects, or adatoms. Amorphous clusters in the top and bottom left corners of Figure 2a,b are likely to be sources of adatoms that migrate on the graphene surface as described earlier. The time sequence shown in Figure 2c was taken from the area marked white in Figure 2b. Adatom #1, marked with a white circle in Figure 2b,c, is stable over the whole time sequence and thus acts as a positional reference within these images. It finally gets detached when the developing hole in the top graphene layer (situated to the bottom right of the atom) reaches the atom position after approximately 5 min of irradiation. In each figure of the time sequence the graphene contrast has also been subtracted. The strong feature of the sputtered edge in the bottom right corner shows the evolution of how single graphene layers can be selectively sputtered by the electron beam as previously observed.[14] Robertson *et al*. show that in the case of an incomplete sheet of graphene residing on FLG a marked increase in contrast can be observed at the edge due to Fresnel interference, which gets stronger with increasing defocus.[34] Over a period of roughly two minutes a number of adatoms (labeled #2–#9 and highlighted with colored circles) appear (full circles) and disappear (dotted circles) in this small sample area. Adatoms #2,

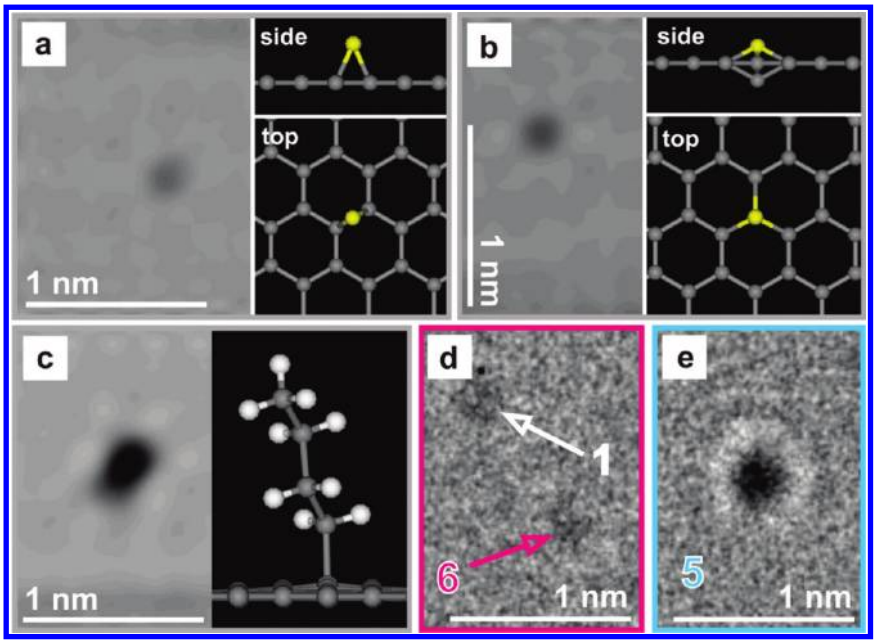

Figure 3. TEM image simulations and corresponding atomic models of (a) a carbon atom adsorbed on the FLG surface in bridge configuration, (b) a carbon adatom in dumbbell configuration, and (c) a carbon chain (C_4H_9) covalently bound to the upper graphene layer and oriented vertical to the graphene layers. Note that the simulations have been carried out using six layers of graphene in the atomic model, but for better clarity only one graphene layer is shown in the model representation; (d, e) HRTEM micrographs of adatoms #1, #6 (27 s) and feature #5 (22 s) as labeled in Figure 2c and appropriately scaled up to match the scale of the image simulations.

#6, #8, and #9 are visible for ≥10 s, and adatom #4 is visible for more than 22 s. The fact that they appear to be stable and well-localized over an extended period of time at room temperature, although the sample is continuously exposed to electron irradiation, suggests that they are chemisorbed.[21] In order to observe these adatoms, they must remain in a fixed position for a significant portion of the duration of the image acquisition, which was typically 1 s in these studies. The feature that appears after 17 s (#5, light blue) may represent a larger molecule or molecular chain due to the stronger contrast as compared to the other adatoms. The contrast gets weaker with time (Figure 2c, 22 to 54 s), which may be due to atoms leaving the chain, and finally, after approximately 70 s the feature disappears. In order to support these statements, TEM image simulations were carried out and are presented in Figure 3.

Figure 3a–c show TEM image simulations of adsorbed species on the top layer of six-layer graphene. The periodic structure of the graphene lattice has been subtracted from the simulated TEM images using a Fourier mask to allow for proper comparison with the HRTEM micrographs. For better clarity only one graphene layer is shown in the respective atomic models in Figure 3a–c. The simulations involve a carbon adatom in bridge configuration[35] (Figure 3a), a carbon adatom in the metastable dumbbell configuration[35] (Figure 3b), and a carbon chain (C_4H_9) covalently attached to the top graphene layer and oriented almost perpendicular to the graphene layers (Figure 3c). Figure 3d,e show HRTEM micrographs of the adatoms #1 and #6 as well as feature #5 from Figure 2c (after 27 and 22 s, respectively) that have been scaled up to match the scale of the image simulations. The dark contrast from the adatoms (Figure 3d) appears to be a little widened as compared to that of the simulated adatoms (Figure 3a,b), which could be due to small-scale oscillations around the anchor point[36] or a slight astigmatism observed in the image. In the case of the TEM simulation of the vertical hydrocarbon chain (Figure 3c) the chain contrast is in good agreement with that of the acquired TEM image (Figure 3e). The assumption that the contrast arising from feature #5 originates from an elongated molecule is corroborated by another time sequence shown in Figure S4 in the Supporting Information, where the formation of an elongated molecule, probably also a hydrocarbon chain, is shown.

Within the inspected field of view gradual transient movement of atoms is not observed. The features are seen to appear and disappear in a discontinuous manner within the short time frame of a few seconds which indicates that they rapidly jump from place to place. However, a period of fixed stability exists that is on the order of seconds, as often observed for systems at the nanoscale, *e.g.*, motion of organic molecules[15] or metallofullerene motion[10] inside carbon nanotubes. After that the atoms either get sputtered off or hop to another energetically favorable position on the graphene sheet, however outside the examined viewing window. Due to the low adatom migration energy of 0.4 eV, carbon atoms generally should move fairly quickly on the graphene surface.[37] Thus detecting their

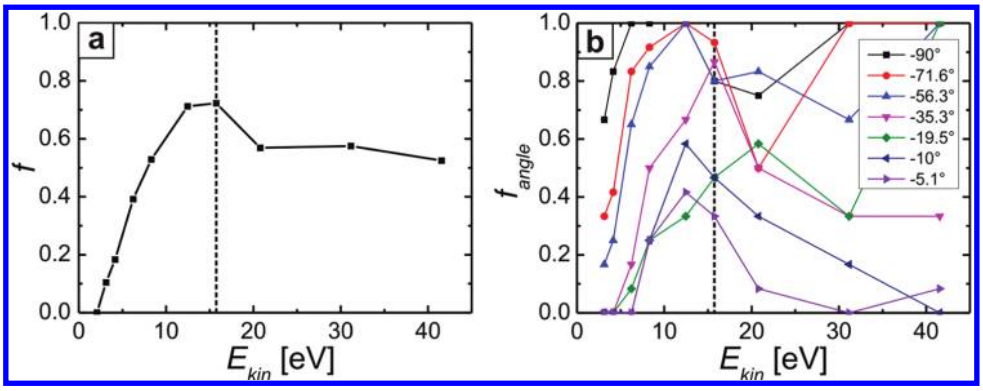

Figure 4. Molecular dynamics: (a) fraction of successful single carbon atom adsorption events, *f*, as a function of the projectile kinetic energy, averaged over all angles of projection; (b) fraction of successful single carbon atom adsorption events at certain projectile angles (with respect to the graphene plane), f_{angle}, as a function of the projectile kinetic energy. The dashed lines in (a) and (b) represent the maximum energy that may be transferred to a carbon atom from an 80 keV electron beam.

motion in TEM at room temperature is thought to be impossible unless they are bound to a defect site, for example a vacancy.[35] Electron irradiation may lead to defect formation in graphitic nanocarbons even at accelerating voltages below the threshold energy for knock-on damage.[38] It has previously been shown that a defect, *e.g.*, a vacancy, becomes a source of a larger hole that develops with time.[14] This is also observed here in Figure 2c with a hole developing in the bottom right corner of the snapshots in the time sequence. The time-dependent dynamics of these defects is distinctly different from what we find with adatoms (and later molecules) which appear and disappear (or move) within a much shorter time frame. While a defect site develops into a two-dimensional hole in the graphene layer, isolated adsorbates often show other morphologies, *i.e.*, point-like or chain-type morphologies, as demonstrated previously.[21] In conjunction with our TEM simulations (*cf.* Figure S5 in the Supporting Information) these findings strongly suggest that black atom contrast arises from adatoms and molecular adsorbates within this study.

In order to understand the conditions in which a carbon atom can be adsorbed, molecular dynamics simulations have been performed using a Tersoff II potential (see Supporting Information for simulation details).[39,40] A single carbon atom is projected toward the graphene surface varying the kinetic energy and angle of projection. Figure 4a shows the fraction of successful single atom adsorption events (*f*) as a function of the kinetic energy (E_{kin}) of the projectile atom averaged over all atom velocities (*i.e.*, not accounting for the angle of projection). Below ~4 eV no successful bonding events are observed. The fraction of successful events reaches a maximum at $E_{kin} \approx 14$ eV, which is close to the maximum energy that may be transferred to a carbon atom under 80 keV electron irradiation ($E_{kin} = 15.73$ eV, as indicated by the dotted line in the figure).[32] The observation that the fraction of successful events falls beyond this threshold is due to significant surface damage at these high energies.

Having established that carbon atoms of considerable kinetic energy can be effectively stopped by the interaction with a graphene sheet, we now need to establish how the projectile angle (with respect to the sheet) may affect these events. Figure 4b shows the fraction of successful adsorption events at certain projectile angles (f_{angle}). As would be expected, there appears to be a strong dependence of the fraction of successful adsorption events on the projectile angle. However, there is still a significant fraction of successful events even at relatively shallow projectile angles (*e.g.*, −5.1°, −10°). In the experimental configuration the less shallow projectile angles correspond to atoms that originate in the vapor above the graphene layers (*i.e.*, vacuum contamination within the TEM), while the shallow angles will generally correspond to atoms that originate from the surface clusters of noncrystalline material (*cf.* Figure 1c). The relative quantities of material obtained from these two sources will depend on both the success rates as a function of projectile angle and the concentration of material available. As a result, although the atoms projected toward the surface are more successful in attaching to the graphene than those fired at more shallow angles, the relatively large local concentration of material in the surface "pools" compared to the vapor more than offsets this effect. This observation therefore supports the assertion that the source of the carbon atoms on the graphene surface may be the clusters of noncrystalline material.

Not only can adatoms be observed on the graphene surface, but also molecules, for example, NMP molecules or hydrocarbon chains, and their motional dynamics can be examined. In Figure 5 a time sequence of images is shown in which a molecule rotates, moves on the FLG surface, and disappears in the end. Figure 5a shows a HRTEM micrograph together with the corresponding FFT as an inset. The graphene contrast has been subtracted in Figure 5b and the time sequence (Figures 5c−f) to enhance the contrast of irregularities as described above. A stable adatom is

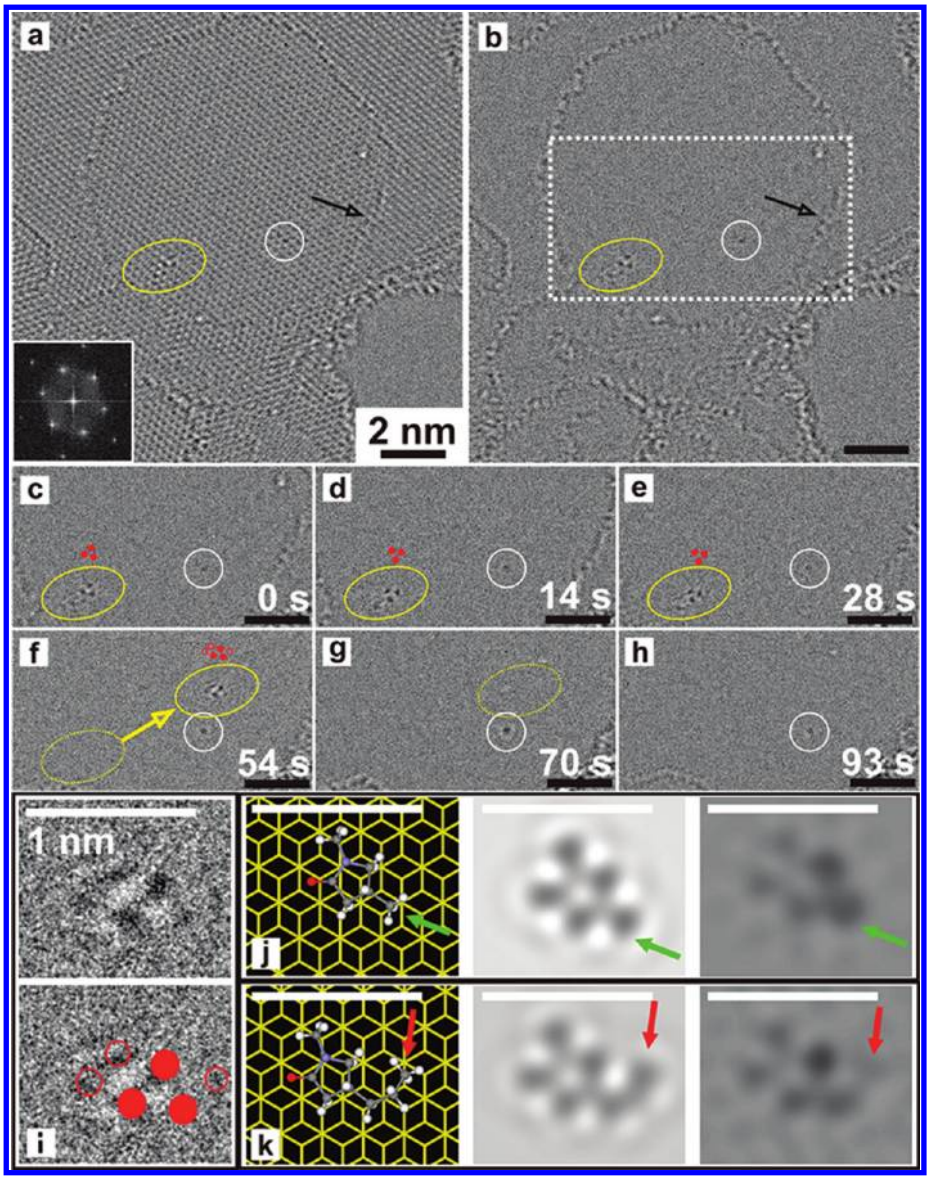

Figure 5. Time series of a moving molecule on FLG: (a) starting image including FFT as inset; (b) starting image with the contrast originating from the FLG flake having been subtracted in order to enhance the contrast of any irregularities, *e.g.*, an adatom (marked white), which acts as positional reference, a graphene step edge (marked with a black arrow), and a larger molecule (marked yellow); (c−h) time series of the region marked white in (b). The "yellow" molecule changes its orientation on the FLG sheet (c, d), moves along the sheet (f), and disappears (g, h). The image acquisition time was 1 s for each frame; (i) enlarged view of (f) together with the respective contrast spot pattern (lower panel); (j) NMP molecule with an added methyl group. Left panel: atomic model; middle panel: TEM image simulation of the isolated molecule (*i.e.*, without graphene); right panel: TEM image simulation of the molecule on top of five-layer graphene; (k) NMP molecule with an added propyl group. Left panel: atomic model; middle panel: TEM simulation of the isolated molecule; right panel: TEM image simulation of the molecule on top of five-layer graphene. The contrast originating from the FLG flake has been subtracted from the simulated TEM images (right panels) as done for the HRTEM micrographs. (Black scale bars correspond to 2 nm, white scale bars to 1 nm.)

marked with a white circle and acts as the positional reference in this time sequence. The black arrow indicates a graphene step edge whose contrast is also strongly enhanced by the removal of the graphene contrast. A larger ensemble of dark contrast spots is highlighted with a yellow ellipse, which most likely is the two-dimensional projection of a molecule. In Figure 5c−e the molecule shows three distinct dark contrast spots that are schematically highlighted with filled red circles just above the actual molecule. A few weaker contrast spots are apparent in close vicinity, especially to the bottom left of the molecule, where it appears to still be attached to the step edge of a graphene layer that has been selectively sputtered in the investigated area, as can clearly be seen in Figure 5b. Figure S6 in the Supporting Information shows magnified views of the images shown in Figure 5c−f together with a dot pattern matching the spot patterns in the TEM micrographs in the lower panel. The three main contrast features are again

highlighted as filled red circles and the clockwise rotation of the molecule is indicated in the figures. The position of these dark contrast spots varies between Figure 5c and d; thus the orientation of the molecule on the FLG flake changes within 14 s. The clockwise rotation between the position of the spot pattern in Figure 5c and d is approximately 60° (*cf.* Figure S6a–c). The ensemble of spots is however located at a fixed position for a period of ≥28 s. After 54 s exposure (Figures 5f and S6d) the molecule has moved to another stable position on the FLG flake and rotated clockwise by another 55°. After 70 s the spots have disappeared from the field of view (Figure 5g). Figure 5i shows an enlarged view of the molecule in Figure 5f. Here it becomes clear that the molecule exhibits at least six dark contrast spots, of which three are in good agreement with the most apparent spots in Figure 5c–e, as highlighted in the lower panel of Figure 5i. Given the fact that the molecule is now definitely detached from the sputtered graphene edge, this spot pattern was investigated by comparison with TEM image simulations (*cf.* Figure S7 in the Supporting Information). In our study NMP serves to exfoliate the graphene and therefore most likely also covers the graphene surface. It has to be expected that many NMP molecules may have been destroyed or may have undergone structural transformation during the electron beam irradiation. However, it is likely that some NMP molecules may survive in nonirradiated areas and later on move into the field of view, being exposed to the electron beam for a significantly shorter time than other sample areas and thus less affected by irradiation damage. Further, the dimensions and the arrangement of the experimentally observed ensemble of contrast spots are in good agreement with contrast patterns obtained from a NMP molecule on graphene generated in TEM simulations. Therefore the TEM simulations were based on an NMP molecule, and extra groups have been added at various positions along the five-membered NMP ring structure.

The left panel of Figure 5j shows an atomic model of an NMP molecule with an extra methyl group attached (1,4-dimethyl-2-pyrolidone). The color code within the structural representation of the molecule is as follows: gray, carbon; white, hydrogen; purple, nitrogen; and red, oxygen. For better visibility the underlying graphene layers are marked yellow in the model. The middle panel of Figure 5j shows a simulated TEM image of the free molecule (*i.e.*, without graphene). The right panel represents an image simulation of the molecule on top of five-layer graphene with the graphene contrast subtracted as in the experimentally observed images. It can be seen that the extra methyl group (marked with a green arrow) gives rise to an extra contrast spot in the simulated TEM image matching a contrast spot in the experimentally observed image. Besides a convergence of the contrast spots, tilting the molecule with respect to the underlying graphene results in a weakening of the contrast of the extra spot when simulating the molecule on top of five-layer graphene (see Figure S7, rows IV–VI, column F for a full set of atomic models and simulated TEM images). Further TEM simulation of a molecule with an added propyl group (marked with a red arrow) is presented in Figure 5k (see also Figure S7, row IX). This 1-methyl-4-propyl-2-pyrolidone molecule provides a very good match of the experimentally observed spot pattern. It would be overreaching to claim that a 1-methyl-4-propyl-2-pyrolidone molecule is indeed present here. Our data do not allow for such a definite answer, as other modified NMP molecules, which have not been tested in TEM simulation, may give rise to a very similar contrast pattern. However, the good agreement between the experimentally observed and the simulated contrast patterns strongly suggests that a structurally modified NMP molecule is seen. Challenges associated with identifying the exact molecular structure also arise from the fact that the contrast profile of the molecule on the graphene sheet is orientation dependent; that is, it changes when translating or rotating the molecule with respect to the underlying graphene. A detailed analysis thereof is presented in Figure S8 in the Supporting Information. Therefore, the contrast profile is not simply a profile of the molecule itself (*cf.* middle panels of Figure 5j,k), but a result of the combination and orientation of the molecule and the graphene lattice. This demonstrates the challenges in obtaining the true contrast profile of a light organic molecule and highlights the limitations of this approach. However, alteration of molecules by addition of extra groups, *i.e.*, growth of a molecule, is not unreasonable even under continuous electron beam irradiation, as will be demonstrated later in the article. Despite these limitations, these studies demonstrate the ability to resolve finer details of the molecular structure of individual molecules compared to previous investigations on light atoms and molecules using conventional microscopes;[21] investigations on elongated molecules, which will be discussed in the following, will further substantiate this.

Furthermore, quicker dynamical motion of molecules can be observed since only a single exposure is necessary to obtain contrast from the adatoms and adsorbed molecules. This is highlighted in the time sequences in Figure 6 and Figure 7 (see also Movie S1 in the Supporting Information). Here the dynamic behavior of a number of molecules and adatoms has been traced over a period of roughly four minutes. An overview TEM micrograph, in which the respective image areas used in Figures 6 and 7 have been highlighted, is presented in Figure S9a in the Supporing Information. In this overview two clusters of amorphous species are visible in close vicinity to the investigated area, which, as suggested from previous

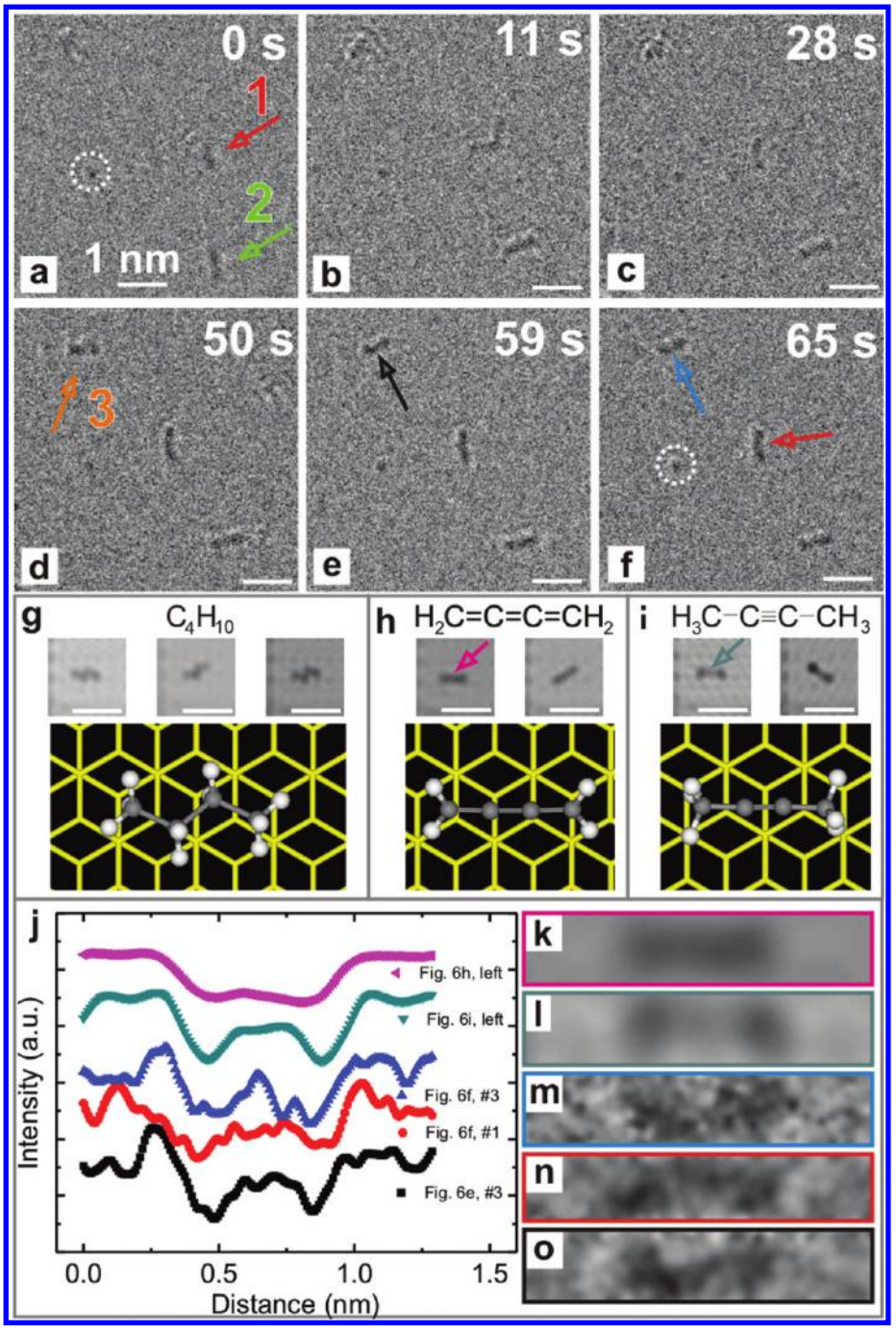

Figure 6. (a–f) Time sequence of the dynamics of elongated molecules on FLG (image acquisition time: 1 s); (g) simulated TEM micrographs of a C_4H_{10} alkane chain in three different positions with respect to the graphene sheet; (h, i) simulated TEM images of a cumulene chain (h) and an alkyne chain (i) in two different positions with respect to the graphene sheet. The atomic models always correspond to the first simulated image shown. The simulated images are scaled appropriately to match the scale of the experimentally observed images. All scale bars correspond to 1 nm; (j) area intensity profiles of the chain molecules marked with colored arrows in (e, f, h, and i); (k–o) magnified and rotated views of these molecules framed with the respective color.

observations and the molecular dynamics simulations (*cf.* Figures 1,2,4b), most probably act as a reservoir of mainly carbon, but also nitrogen and oxygen atoms for the formation of the molecules visible in Figures 6 and 7. Sample drift has been taken into account by accurately realigning the image using a reference marker. In these time sequences (Figures 6 and 7) the atom marked with a white circle represents the positional reference in both figures, which is also highlighted in Figure S9a in the Supporting Information. Although in a TEM micrograph one sees only a two-dimensional projection of a three-dimensional structure, we are confident that the observed molecules are chain molecules, most likely hydrocarbon chains. We have

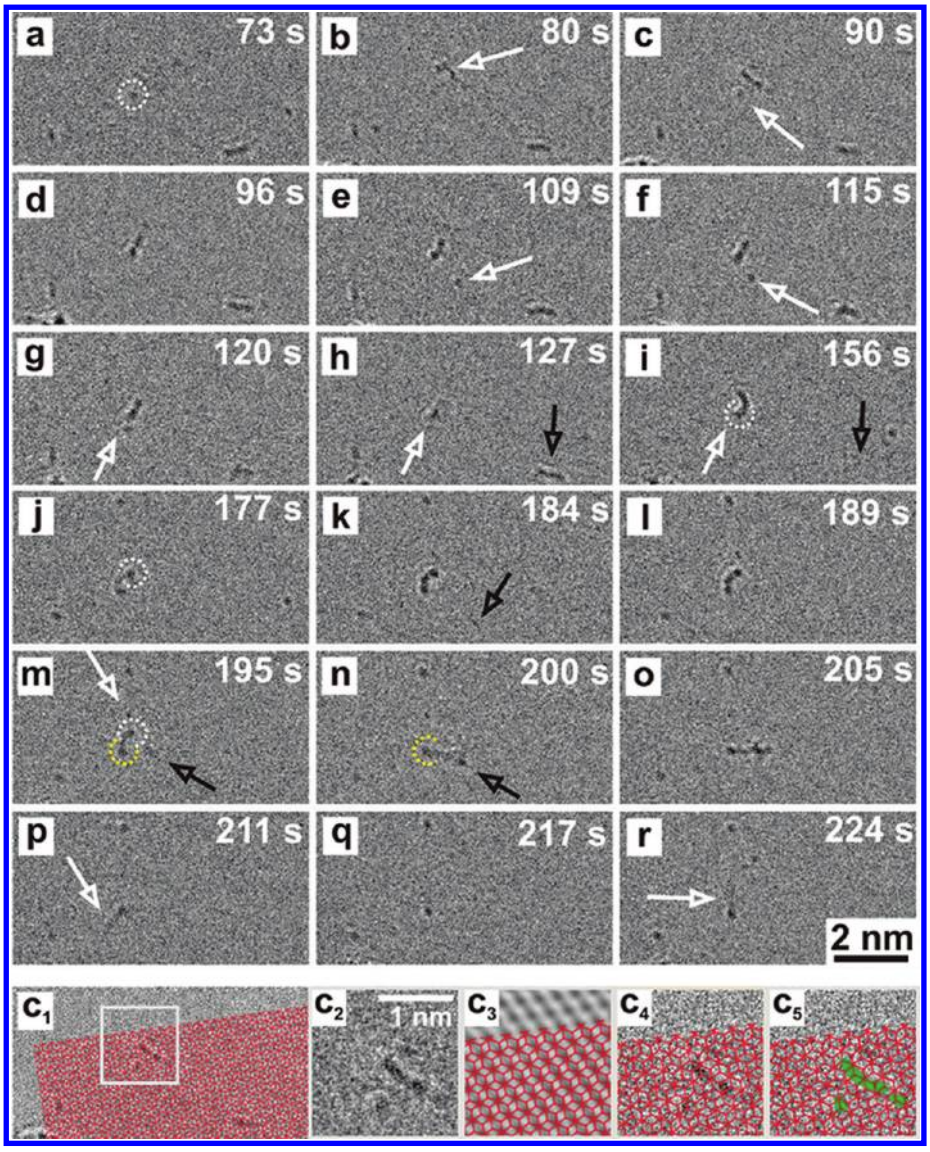

Figure 7. (a−r) Time sequence of the growth and the dynamic behavior of a chain molecule (image acquisition time: 1 s). The feature circled white in (a) is the same positional reference as in Figure 6. It further is the anchoring point for a molecule (Figure 7d) that swings around it. Later the molecule anchors to a point further down within the investigated area as highlighted by the yellow semicircle (m, n); (c_1−c_5) Positional analysis of molecular features on the FLG *xy*-plane: (c_1) an AB stacked atomic FLG model is superimposed on frame c; (c_2−c_5) magnified views of the section marked with a gray square in (c_1); (c_2) molecular contrast only; (c_3) contrast of the FLG sheet with the molecular contrast subtracted as utilized to superimpose the atomic model; (c_4) molecular contrast and atomic model; (c_5) molecular contrast highlighted in green.

monitored these molecules over approximately four minutes. Within this time frame most of the features appear elongated at all times even though they are moving and possibly rotating around their length axes. If extra groups were present, we would expect to observe them during movement of the molecule.

In the first part of the time sequence (Figure 6) two chain molecules (#1 and #2) are visible that appear to be straight and oriented lengthwise in the first frame (marked with arrows in Figure 6a). After 11 s (Figure 6b) molecule #1 appears to be stronger in contrast and longer and shows an elbow-like bend with a projected angle of approximately 114° (measured value). This kink suggests that the atom at the kink (that is carbon, oxygen, or nitrogen) is sp^2- or sp^3-hybridized. The straight chains on the other hand suggest sp-hybridization. Molecule #2 has rotated around its upper end and is now oriented sideways. It keeps this position and approximate orientation for the duration of the whole time sequence. Indeed it disappears only after 156 s (Figure 7h,i, black arrow). In direct comparison, molecule #1 shows stronger dynamics. After 28 s the elbow-tip appears to have moved ∼0.7 nm toward the reference atom and slightly rotated anticlockwise. The contrast of the "forearm" can just be seen in this image (Figure 6c). In the following images the molecule seems to be shorter, but exhibits a darker contrast. In this position the molecule is stable for at least

another 15 s (until 65 s of total exposure, Figure 6f). After 73 s exposure (Figure 7a) it is no longer visible at this position.

We conducted TEM image simulations in order to provide deeper insight into what these elongated regions of contrast could possibly be, in other words, what atomic structures could give rise to a similar contrast. The structures tested in TEM simulation here have not deliberately been placed on the sample, but they could easily form from the carbonaceous residue. Previous studies by others using conventional TEM suggested hydrocarbon chains, alkanes or alkenes, to reside on the graphene surface.[21] Therefore, since the observed structures often appear to be elongated and since a large amount of carbon and hydrogen atoms can be expected to be within the residue, hydrocarbon chains are highly likely candidates. Consequently alkane, cumulene, and alkyne chains of different lengths served as test molecules. From simulations of different hydrocarbon chains, that is, butane (Figure 6g, C_4H_{10}, alkane), butatriene (Figure 6h, C_4H_4, cumulene), and dimethylacetylene (Figure 6i, C_4H_6, alkyne) it can be derived that the experimentally observed chain molecules (or molecular segments in the case of the elbow-like feature) consist of a minimum of four or five carbon atoms in the chain (*cf.* Figure S9 in the Supporting Information). In the simulations the molecules were always placed flat onto the graphene surface; therefore their projected length in the simulated micrographs is maximized. This of course may not be the case for the experimentally observed molecules. They may be at an angle with respect to the underlying graphene, which inevitably would lead to a shorter two-dimensional projection in the TEM micrograph. However, $\pi-\pi$-interaction between the molecules and the graphene should lead to a preferential flattening of the molecule.

Further, the chains have been simulated in different positions with respect to the plane of the FLG sheet; that is, the chains have been rotated around the graphene *c*-axis as a whole as well as rotated along their principal axis. While the double and triple bonds in cumulene and alkyne are rigid due to the π-orbitals overlapping, leading to straight molecules (Figure 6h,i), the spatial arrangement of the alkane chain is governed by the tetrahedral sp^3-orbitals. This difference can also be clearly made out in the image simulations, where the alkane chain always causes a zigzag contrast (Figure 6g), whereas the cumulene and alkyne chains appear as straight lines. Further the TEM simulations reveal that the contrast of the cumulene chain hardly varies along the molecule's length (Figure 6h), while in the case of the alkyne chain the methyl end groups lead to a broadening as well as an increase of the chain's contrast (Figure 6i). The examined molecules appear to be rather straight, which suggests sp-hybridization.

Furthermore, the molecules show increased contrast toward their ends. Figure 6j summarizes the quantitative analysis of the area intensity profiles along the length of these molecules. The intensity profiles plotted in Figure 6j correspond to the simulated molecules marked with a colored arrow in Figure 6h,i as well as the experimentally obtained micrographs of molecules #1 and #3, as marked with colored arrows in Figure 6e,f. For improved visual clarity, magnified and rotated views of these molecules are presented in Figure 6k–o and framed with the corresponding color of the arrow. While the area intensity profile of the simulated cumulene chain (pink) resembles a plateau, the profile of the simulated alkyne chain (green) shows two distinct minima. These minima are also clearly obtained in the intensity profiles of the HRTEM micrographs. Therefore, the stronger contrast toward the molecules' ends may be referred to as methyl end groups (*cf.* Figure 6i). We further investigated whether the molecules are aligned with respect to a low-indexed armchair or zigzag direction of the underlying few-layer graphene. At times, the molecules appeared to be aligned with either direction; for example in Figure 6a both molecules appeared to be oriented along an armchair direction (as exemplarily highlighted in the inset in Figure S9b in the Supporting Information). However, conclusive evidence for a preferred arrangement was not obtained from our statistics within the data sets.

The second part of the time sequence is presented in Figure 7a–r. In addition, Figure 8 gives a schematic illustration of the observed dynamic behavior of the molecules. As mentioned above, the molecule that was located in the middle of the field of view (Figure 6f) seems to have disappeared after 73 s (Figure 7a). However, after just seven more seconds (Figure 7b) a new feature appears just above the reference atom (white arrow) in close vicinity to the previous location of the molecule. Therefore, either the molecule has desorbed and another molecule was released from the reservoir or the molecule was moving from its original position to the position it has adopted in Figure 7b, which is more likely. This suggests that a quick movement occurred while Figure 7a was acquired (1 s exposure time), since the molecule can hardly be made out in this frame. In Figure 7c the molecule then moves toward the reference feature and anchors at the defect site after another six seconds (Figure 7d and schematically illustrated in Figure 8a–c). At the reference site dangling bonds may be available and reaction with an unsaturated carbon atom within the hydrocarbon chain can lead to a stable bond at this location. The molecule, now anchored, swings around this fixed point for about 100 s (Figure 7m, Figure 8d). In Figure 7h the dynamical motion is so quick that the molecule cannot be detected within the camera exposure time of 1 s. During this period (Figure 7d–m) other adatoms move toward the chain molecule. Frames 7e and 7f show the approach of an adatom

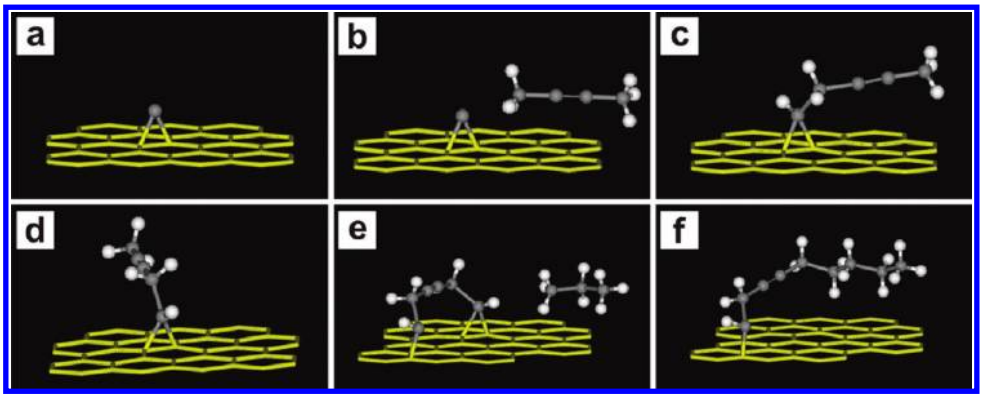

Figure 8. Schematic illustration of the molecular movement observed *via* TEM (*cf.* Figure 7). (a) Carbon atom on top graphene layer adsorbed in bridge configuration; (b) alkyne chain approaching the defect site; (c) alkyne chain is attached to the adatom; (d) alkyne chain swings around the anchor point; (e) free end of the alkyne chain is trapped at another carbon adatom; a short alkane (C_3H_8) reaches the site; (f) alkane chain reacts with the adsorbed molecule, thereby detaching it from the first anchor point.

that is subsequently attached to the molecule (Figure 7g). In Figure 7i a darker feature (to the right of the black arrow), possibly a vertically oriented molecule (cf. Figure 3c), is visible, but has disappeared after 11 s (Figure 7k). Instead some blurred features can be seen in Figure 7k,m (black arrows) moving toward the swinging molecule (schematic in Figure 8e). This feature appears to attach at the top of the molecule (Figure 7m), possibly detaching the molecule from its anchor point (Figure 7n, Figure 8f). In the following figures it can clearly be seen that the anchor point has now changed to a slightly lower location within the frame (yellow semicircle). The molecule, now much longer, swings around this new anchor point, leaving only a faint contrast in the following frames (white arrows in Figure 7p,r). Similar to the dynamic behavior of the adatoms (cf. Figure 2), the molecules in Figures 6 and 7 show positions of fixed stability between varying motional action, *i.e.*, motion on the graphene surface (*xy*-plane) or swinging around the anchor point. These periods of stability can easily be captured within our image acquisition time of 1 s, as they occur within a time scale of seconds or even minutes.[10,15,21] The motional action or molecular motion in between those periods of fixed stability will occur on a more rapid time scale (down to femtoseconds) and may be detected by other methods, such as UEM, yet with reduced spatial resolution.[18]

Figure $7c_1$–c_5 further demonstrate how the positional analysis of the molecular features on the graphene *xy*-plane was carried out throughout the investigation. Frame 7c of the time sequence is used as an example. In Figure $7c_1$ the atomic model of AB stacked FLG is superimposed on frame 7c to identify the orientation of the molecule with respect to the FLG sheet and the *xy* position of its anchor point. Figure $7c_2$–c_5 show magnified views of the section marked with a gray square in Figure $7c_1$. Here, Figure $7c_2$ shows the image containing just the molecular contrast, while Figure $7c_3$ shows the contrast of the FLG lattice with the molecular contrast erased (*cf.* Figure S3, *i.e.*, inverse FFT of mask), as utilized to superimpose the atomic model. Figure $7c_4$,c_5 then show the molecular contrast together with the atomic model as well as a green mask highlighting the features. From this analysis it can be concluded that the molecule is not anchored at a specific lattice site of the underlying FLG sheet. Further, the molecule's orientation does not follow a low indexed direction in the FLG lattice as indicated above.

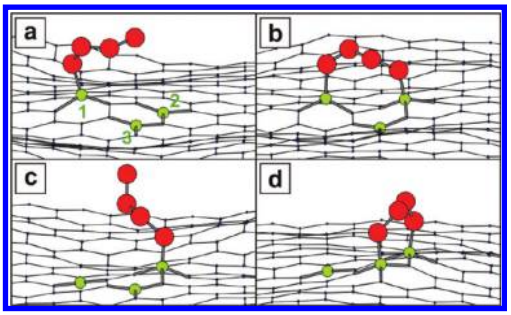

Figure 9. Molecular graphics "snapshots" of the motion of a four-atom carbon chain across a graphene layer. The chain initially rotates about site 1 (a) before forming a "dual-tether" complex (b), where the chain end bonds to site 2. The re-energized chain rotates about site 2 (c) and finally forms a second dual-tether complex at site 3 (d).

To investigate the possible molecular chain motion observed experimentally, molecular dynamics simulations are performed in which a four-atom chain is adsorbed to a single graphene sheet and then energized (reflecting the potential use of the electron beam). Figure 9 shows molecular graphics "snapshots" of the carbon chain on the graphene sheet. The chain is initially tethered at site 1 (Figure 9a). On energizing, the chain rotates until, after $t \approx 1.6$ ps, the chain end attaches to the surface at site 2 (Figure 9b), forming a "dual-tether" complex. The attachment to site 2 effectively dissipates the "excess" chain kinetic energy to

the graphene sheet. On re-energizing the chain about tether point 2, the bond to the original tether is broken and the atom now rotates around site 2 (Figure 9c). After a further $t \approx 1.5$ ps the chain attaches at site 3 and another dual-tether complex is formed (Figure 9d). These molecular dynamics studies highlight the feasibility of molecular chain motion on a graphene surface and give support to the experimental observations.

CONCLUSION

We have monitored and analyzed the movement of atoms and molecules adsorbed on electron beam cleaned FLG. Making use of HOPG as carbon precursor as well as NMP as solvent for liquid phase exfoliation ensures that the adsorbates predominantly consist of light atoms. The adatoms are found to get trapped on the graphene surface, remain stably localized for some time, at least long enough to be imaged in single exposures with typically 1 s acquisition time, and suddenly disappear again. We showed that electron beam irradiation led to several small atomic clusters fusing together to form larger molecular chains on the surface of FLG. Furthermore, we observed such a molecular chain, most probably a hydrocarbon chain, getting anchored at a site and swinging around this tether point.

Our findings highlight how beneficial it is to make use of aberration-corrected LV-HRTEM for the investigation of light molecules, *i.e.*, to simultaneously obtain atomic structure information as well as their motional behavior at room temperature. In comparison to conventional TEM greater detail of the molecular structure can be achieved, and with the support of TEM image simulations more accurate conclusions on the actual structure of the molecules can be drawn. Here, contrast intensity profile analysis of the experimentally observed chains and the simulated cumulene and alkyne chains provided assurance that the increased contrast toward the end of the molecules may originate from methyl end groups. Furthermore, by overlaying an atomic model, atomic-structure information of the FLG can easily be utilized to identify the adsorbates' positions as well as their orientation/alignment with respect to the underlying FLG sheet.

Our results also indicate that in-plane motion of the adatoms and molecules on the graphene surface is feasible. The adatom source appears to be the carbonaceous clusters of residual solvent species rather than contaminant atoms from the TEM vacuum. While the number of successful adsorption events is an order of magnitude higher for steep projectile angles as compared to shallow angles, as derived from molecular dynamics simulations, the amount of available carbon in the microscope's atmosphere that could end up in the examined region is significantly smaller than in the clusters, which corroborates the scenario of the clusters being the major source of adatoms and molecules.

We further demonstrated that the dynamic behavior can be detected through single-shot exposure even for light molecules that do not contain strong scatterers, *i.e.*, that mainly consist of carbon and hydrogen. In the future the technique will allow for the observation of even quicker dynamics, on the order of 0.1 s and less.[14] However, as outlined in this article, great care has to be taken when using graphene as a substrate for high-resolution imaging of molecules, since unwanted surface contaminants may compromise the investigation.

METHODS

Graphene and FLG sheets were prepared by placing small flakes of highly ordered pyrolytic graphite in *N*-methyl-2-pyrrolidone solvent and sonicating for 2 h as described elsewhere.[28] The solution was left to settle for 1 h to allow thicker graphite sheets to sediment to the bottom of the vial. The top third of the dispersion was pipetted off and placed in a clean vial. For TEM sample preparation a drop from the dispersion was deposited onto a 400 mesh lacey carbon coated TEM grid, washed in methanol, and then left to dry. The graphene sheets deposited in this way typically comprised 1−10 graphene layers. NMP consists of carbon, nitrogen, and oxygen atoms, and HOPG contains very little metallic impurities as compared to other graphite sources. Therefore the debris on the surface of the FLG flakes should contain only light atoms, that is, carbon, nitrogen, oxygen, and hydrogen.

LV-HRTEM was carried out using the Oxford-JEOL JEM-2200MCO high-resolution transmission electron microscope, equipped with probe and image aberration correctors and operated at an acceleration voltage of 80 kV to minimize sample damage by the electron beam. The image acquisition time was typically 1 s. For TEM image simulations the DS ViewerPro software was used to generate rectangular supercell structures consisting of few-layer graphene (5 or 6 layers) as well as adatoms, molecules, defects, and carbon chains on its surface. The image simulations of these structures were performed using JEMS software, which implements the multislice algorithm. TEM simulation parameters were set to an accelerating voltage of 80 kV, a spherical aberration coefficient (C_S) of −0.01 mm, a chromatic aberration (C_C) of 0.8 mm, a fifth-order spherical aberration coefficient (C_5) of 1 mm, an energy spread of 0.3 eV, a defocus of 1 nm, and a defocus spread of 10 nm, which is sufficient to resolve the $(10\bar{1}0)$ lattice fringes (0.21 nm) in graphite.

Details on the molecular dynamics simulations can be found in the Supporting Information.

Acknowledgment. F.S. thanks the Alexander von Humboldt Foundation, the BMBF, and the EPSRC (EP/F048009/1). J.H.W. thanks the Royal Society, the Glasstone Fund, and Brasenose College for support.

Supporting Information Available: Details on the molecular dynamics simulations. Process of determining the number of graphene layers. Determination of the rate of atoms lost during electron irradiation. Details on the procedure(s) of image processing. Time series of the formation of an elongated molecule. Additional analysis of the time sequence presented in Figure 5, including enlarged TEM micrographs and detailed TEM simulation data on NMP-like molecules. Determination of length and orientation of the chain molecules (experiment and TEM simulation). Movie assembled from frames of the time sequences to visualize the dynamic behavior of the molecules. This material is available free of charge *via* the Internet at http://pubs.acs.org.

REFERENCES AND NOTES

1. Leigh, D. A.; Zerbetto, F.; Kay, E. R. Synthetic Molecular Motors and Mechanical Machines. *Angew. Chem., Int. Ed.* **2007**, *46*, 72–191.
2. Moresco, F.; Meyer, G.; Rieder, K.-H.; Tang, H.; Gourdon, A.; Joachim, C. Recording Intramolecular Mechanics during the Manipulation of a Large Molecule. *Phys. Rev. Lett.* **2001**, *87*, 088302.
3. Minko, S.; Kiriy, A.; Gorodyska, G.; Stamm, M. Single Flexible Hydrophobic Polyelectrolyte Molecules Adsorbed on Solid Substrate: Transition between a Stretched Chain, Necklace-like Conformation and a Globule. *J. Am. Chem. Soc.* **2002**, *124*, 3218–3219.
4. Liu, Z.; Suenaga, K.; Iijima, S. Imaging the Structure of an Individual C_{60} Fullerene Molecule and Its Deformation Process Using HRTEM with Atomic Sensitivity. *J. Am. Chem. Soc.* **2007**, *129*, 6666–6667.
5. Girit, Ç. Ö.; Meyer, J. C.; Erni, R.; Rossell, M. D.; Kisielowski, C.; Yang, L.; Park, C.-H.; Crommie, M. F.; Cohen, M. L.; Louie, S. G.; *et al*. Graphene at the Edge: Stability and Dynamics. *Science* **2009**, *323*, 1705–1708.
6. Börrnert, F.; Börrnert, C.; Gorantla, S.; Liu, X.; Bachmatiuk, A.; Joswig, J.-O.; Wagner, F. R.; Schäffel, F.; Warner, J. H.; Schönfelder, R.; *et al*. Single-Wall-Carbon-Nanotube/Single-Carbon-Chain Molecular Junctions. *Phys. Rev. B* **2010**, *81*, 085439.
7. Gorantla, S.; Börrnert, F.; Bachmatiuk, A.; Dimitrakopoulou, M.; Schönfelder, R.; Schäffel, F.; Thomas, J.; Gemming, T.; Borowiak-Palen, E.; Warner, J. H.; *et al*. In Situ Observations of Fullerene Fusion and Ejection in Carbon Nanotubes. *Nanoscale* **2010**, *2*, 2077–2079.
8. Krasheninnikov, A. V.; Banhart, F. Engineering of Nanostructured Carbon Materials with Electron or Ion Beams. *Nat. Mater.* **2007**, *6*, 723–733.
9. Khlobystov, A. N.; Porfyrakis, K.; Kanai, M.; Britz, D. A.; Ardavan, A.; Shinohara, H.; Dennis, T. J. S.; Briggs, G. A. D. Molecular Motion of Endohedral Fullerenes in Single-Walled Carbon Nanotubes. *Angew. Chem., Int. Ed.* **2004**, *43*, 1386–1389.
10. Warner, J. H.; Watt, A. A. R.; Ge, L.; Porfyrakis, K.; Akachi, T.; Okimoto, H.; Ito, Y.; Ardavan, A.; Montanari, B.; Jefferson, J. H.; *et al*. Dynamics of Paramagnetic Metallofullerenes in Carbon Nanotube Peapods. *Nano Lett.* **2008**, *8*, 1005–1010.
11. Koshino, M.; Solin, N.; Tanaka, T.; Isobe, H.; Nakamura, E. Imaging the Passage of a Single Hydrocarbon Chain Through a Nanopore. *Nat. Nanotechnol.* **2008**, *3*, 595–597.
12. Gorantla, S.; Avdoshenko, S.; Börrnert, F.; Bachmatiuk, A.; Dimitrakopoulou, M.; Schäffel, F.; Schönfelder, R.; Thomas, J.; Gemming, T.; Warner, J. H.; *et al*. Enhanced $\pi-\pi$ Interactions Between a C_{60} Fullerene and a Buckle Bend on a Double-Walled Carbon Nanotube. *Nano Res.* **2010**, *3*, 92–97.
13. Shiozawa, H.; Pichler, T.; Grüneis, A.; Pfeiffer, R.; Kuzmany, H.; Liu, Z.; Suenaga, K.; Kataura, H. A Catalytic Reaction Inside a Single-Walled Carbon Nanotube. *Adv. Mater.* **2008**, *20*, 1443–1449.
14. Warner, J. H.; Rümmeli, M. H.; Ge, L.; Gemming, T.; Montanari, B.; Harrison, N. M.; Büchner, B.; Briggs, G. A. D. Structural Transformations in Graphene Studied with High Spatial and Temporal Resolution. *Nat. Nanotechnol.* **2009**, *4*, 500–504.
15. Koshino, M.; Tanaka, T.; Solin, N.; Suenaga, K.; Isobe, H.; Nakamura, E. Imaging of Single Organic Molecules in Motion. *Science* **2007**, *316*, 853.
16. Liu, Z.; Yanagi, K.; Suenaga, K.; Kataura, H.; Iijima, S. Imaging the Dynamics Behaviour of Individual Retinal Chromophores Confined in Carbon Nanotubes. *Nat. Nanotechnol.* **2007**, *2*, 422–425.
17. Somada, H.; Hirahara, K.; Akita, S.; Nakayama, Y. A. Molecular Linear Motor Consisting of Carbon Nanotubes. *Nano Lett.* **2009**, *9*, 62–65.
18. Park, H. S.; Baskin, J. S.; Kwon, O.-H.; Zewail, A. H. Atomic-Scale Imaging in Real and Energy Space Developed in Ultrafast Electron Microscopy. *Nano Lett.* **2007**, *7*, 2545–2551.
19. Lee, Z.; Jeon, K.-J.; Dato, A.; Erni, R.; Richardson, T. J.; Frenklach, M.; Radmilovic, V. Direct Imaging of Soft-Hard Interfaces Enabled by Graphene. *Nano Lett.* **2009**, *9*, 3365–3369.
20. McBride, J. R.; Lupini, A. R.; Schreuder, M. A.; Smith, N. J.; Pennycook, S. J.; Rosenthal, S. J. Few-Layer Graphene as a Support Film for Transmission Electron Microscopy Imaging of Nanoparticles. *ACS Appl. Mater. Interfaces* **2009**, *1*, 2886–2892.
21. Meyer, J. C.; Girit, Ç. Ö.; Crommie, M. F.; Zettl, A. Imaging and Dynamics of Light Atoms and Molecules on Graphene. *Nature* **2008**, *454*, 319–322.
22. Jin, C.; Lan, H.; Peng, L.; Suenaga, K.; Iijima, S. Deriving Carbon Atomic Chains from Graphene. *Phys. Rev. Lett.* **2009**, *102*, 205501.
23. Wilson, N. R.; Pandey, P. A.; Beanland, R.; Young, R. J.; Kinloch, I. A.; Gong, L.; Liu, Z.; Suenaga, K.; Rourke, J. P.; York, S. J.; *et al*. Graphene Oxide: Structural Analysis and Application as a Highly Transparent Support for Electron Microscopy. *ACS Nano* **2009**, *3*, 2547–2556.
24. Sloan, J.; Liu, Z.; Suenaga, K.; Wilson, N. R.; Pandey, P. A.; Perkins, L. M.; Rourke, J. P.; Shannon, I. J. Imaging the Structure, Symmetry, and Surface-Inhibited Rotation of Polyoxometalate Ions on Graphene Oxide. *Nano Lett.* **2010**, *10*, 4600–4606.
25. Chuvilin, A.; Kaiser, U.; Bichoutskaia, E.; Besley, N. A.; Khlobystov, A. N. Direct Transformation of Graphene to Fullerene. *Nat. Chem.* **2010**, *2*, 450–453.
26. Gan, Y.; Sun, L.; Banhart, F. One- and Two-Dimensional Diffusion of Metal Atoms in Graphene. *Small* **2008**, *4*, 587–591.
27. Dato, A.; Radmilovic, V.; Lee, Z.; Phillips, J.; Frenklach, M. Substrate-Free Gas-Phase Synthesis of Graphene Sheets. *Nano Lett.* **2008**, *8*, 2012–2016.
28. Hernandez, Y.; Nicolosi, V.; Lotya, M.; Blighe, F. M.; Sun, Z.; De, S.; McGovern, I. T.; Holland, B.; Byrne, M.; Gun'ko, Y. K.; *et al*. High-Yield Production of Graphene by Liquid-Phase Exfoliation of Graphite. *Nat. Nanotechnol.* **2008**, *3*, 563–568.
29. Warner, J. H.; Schäffel, F.; Rümmeli, M. H.; Büchner, B. Examining the Edges of Multi-Layer Graphene Sheets. *Chem. Mater.* **2009**, *21*, 2418–2421.
30. Smith, B. W.; Luzzi, D. E. Electron Irradiation Effects in Single Wall Carbon Nanotubes. *J. Appl. Phys.* **2001**, *90*, 3509–3515.
31. Schäffel, F.; Wilson, M.; Bachmatiuk, A.; Rümmeli, M. H.; Queitsch, U.; Rellinghaus, B.; Briggs, G. A. D.; Warner, J. H. Atomic Resolution Imaging of the Edges of Catalytically Etched Suspended Few Layer Graphene. *ACS Nano* **2011**, *5*, 1975–1983.
32. Egerton, R. F.; Li, P.; Malac, M. Radiation Damage in the TEM and SEM. *Micron* **2004**, *35*, 399–409.
33. Crozier, P. A.; McCartney, M. R.; Smith, D. J. Observation of Exit Surface Sputtering in TiO_2 Using Biased Secondary Electron Imaging. *Surf. Sci.* **1990**, *237*, 232–240.
34. Robertson, A. W.; Bachmatiuk, A.; Wu, Y. A.; Schäffel, F.; Rellinghaus, B.; Büchner, B.; Rümmeli, M. H.; Warner, J. H. Atomic Structure of Interconnected Few-Layer Graphene Domains. *ACS Nano* **2011**, *5*, 6610–6618.
35. Banhart, F.; Kotakoski, J.; Krasheninnikov, A. V. Structural Defects in Graphene. *ACS Nano* **2011**, *5*, 26–41.
36. Cretu, O.; Krasheninnikov, A. V.; Rodríguez-Manzo, J. A.; Sun, L.; Nieminen, R. M.; Banhart, F. Migration and Localization of Metal Atoms on Strained Graphene. *Phys. Rev. Lett.* **2010**, *105*, 196102.
37. Lehtinen, P. O.; Foster, A. S.; Ayuela, A.; Krasheninnikov, A. V.; Nordlund, K.; Nieminen, R. M. Magnetic Properties and Diffusion of Adatoms on a Graphene Sheet. *Phys. Rev. Lett.* **2003**, *91*, 017202.
38. Warner, J. H.; Schäffel, F.; Zhong, G.; Rümmeli, M. H.; Büchner, B.; Robertson, J.; Briggs, G. A. D. Investigating the Diameter-Dependent Stability of Single-Walled Carbon Nanotubes. *ACS Nano* **2009**, *3*, 1557–1563.
39. Tersoff, J. New Empirical Approach for the Structure and Energy of Covalent Systems. *Phys. Rev. B* **1988**, *37*, 6991–7000.
40. Bishop, C. L.; Wilson, M. The Energetics of Inorganic Nanotubes. *Mol. Phys.* **2008**, *106*, 1665–1674.